Effect of Alkyl Chain Unsaturation and Cholesterol Intercalation on Oxygen Transport in Membranes: A Pulse ESR Spin Labeling Study[†]

Witold K. Subczynski,*[,‡,§] James S. Hyde,[‡] and Akihiro Kusumi*[,‡,‖]

National Biomedical ESR Center, Department of Radiology, Medical College of Wisconsin, Milwaukee, Wisconsin 53226, Biophysics Department, Institute of Molecular Biology, Jagiellonian University, 31-120 Krakow, Poland, and Department of Pure and Applied Sciences, College of Arts and Sciences, The University of Tokyo, Meguro-ku, Tokyo 153, Japan

Received February 21, 1991; Revised Manuscript Received May 29, 1991

ABSTRACT: Transport and diffusion of molecular oxygen in phosphatidylcholine (PC)–cholesterol membranes and their molecular mechanism were investigated. A special attention was paid to the molecular interaction involving unsaturated alkyl chains and cholesterol. Oxygen transport was evaluated by monitoring the bimolecular collision rate of molecular oxygen and the lipid-type spin labels, tempocholine phosphatidic acid ester, 5-doxylstearic acid, and 16-doxylstearic acid. The collision rate was determined by measuring the spin-lattice relaxation times (T_1's) in the presence and absence of molecular oxygen with long-pulse saturation–recovery ESR techniques. In the absence of cholesterol, incorporation of *either a cis or trans* double bond at the C9–C10 position of the alkyl chain *decreases* oxygen transport at all locations in the membrane. The activation energy for the translational diffusion of molecular oxygen in the absence of cholesterol is 3.7–6.5 kcal/mol, which is comparable to the activation energy theoretically estimated for kink migration or C–C bond rotation of alkyl chains [Träuble, H. (1971) *J. Membr. Biol. 4*, 193–208; Pace, R. J., & Chan, S. I. (1982) *J. Chem. Phys. 76*, 4241–4247]. Intercalation of cholesterol in saturated PC membranes reduces oxygen transport in the headgroup region and the hydrophobic region near the membrane surface but little affects the transport in the central part of the bilayer. In unsaturated PC membranes, intercalation of cholesterol also reduces oxygen transport in and near the headgroup regions. In contrast, it *increases* oxygen transport in the middle of the bilayer. On the basis of these observations, a model for the mechanism of oxygen transport in the membrane is proposed in which oxygen molecules reside in vacant pockets created by gauche–trans isomerization of alkyl chains and the structural nonconformability of neighboring lipids, unsaturated PC and cholesterol in particular, and oxygen molecules jump from one pocket to the adjacent one or move along with the movement of the pocket itself. The presence of cholesterol decreases oxygen permeability across the membrane in all membranes used in this work in spite of the increase in oxygen transport in the central part of unsaturated PC–cholesterol membranes because cholesterol decreases oxygen transport in and near the headgroup regions, where the major barriers for oxygen permeability are located. Oxygen gradients across the membranes of the cells and the mitochondria are evaluated. Arguments are advanced that oxygen permeation across the protein-rich mitochondrial membranes can be a rate-limiting step for oxygen consumption under hypoxic conditions in vivo.

Transport[1] of small molecules within and across the cell membrane is one of the principal functions of cellular membranes (Adam & Delbrück, 1968). In particular, transport and diffusion in the lipid domain of the membrane are of fundamental importance since the lipid bilayers provide cells and cellular organelles with major diffusion barriers (Albert et al., 1988). A substantial body of data on the permeability of various molecules has been accumulating (Anderson, 1978; Finkelstein, 1984; Walter & Gutknecht, 1986; Subczynski et al., 1989). However, very little is known on the *molecular mechanism* of transport within and across the lipid bilayer membranes.

Molecular models for diffusion and transport of small molecules in the membrane have been proposed (Träuble, 1971; Pace & Chan, 1982). According to Träuble (1971), small molecules enter the free volume formed by the kink

conformation in the phospholipid alkyl chains and migrate across the membrane as the kink migrates. The concentration and the diffusion coefficient of the kink within hydrocarbon region of the membrane were estimated to be about 8 M and 10^{-5} cm^2/s, respectively. Pace and Chan (1982) proposed that diffusion of small molecules occurs by hopping of these molecules between adjacent kinks. In this mechanism, molecular diffusion takes place through kink formation of adjacent chains, in contrast to kink migration along one acyl chain in Träuble's model. Evaluated activation energy for the kink migration is 4.8 kcal/mol (Träuble, 1971) and 3.1 kcal/mol for bond rotation (isomerization) (Pace & Chan, 1982). In order to advance such studies on the molecular mechanism of diffusion and transport of small molecules in the lipid bilayer membranes, further experimental investigation is needed.

Recently, we have been studying the transport of small paramagnetic molecules, molecular oxygen (O$_2$, MW = 32) and a copper square-planar complex [[3-ethoxy-2-oxobutyr-

[1] In the present paper, the word "transport" indicates the product of the (local) translational diffusion coefficient and the (local) concentration of small molecules in the membrane. Thus, "transport" is used here in its basic physical meaning. This quantity is important because it is directly related to the bimolecular reaction rate due to the proportionality to the bimolecular collision rate. Active transport across the membrane is not the subject of this paper.

aldehyde bis(N^4,N^4-dimethylthiosemicarbazonato)]copper(II) called CuKTSM$_2$,[2] MW = 394], within and across the lipid bilayer membranes (Subczynski & Hyde, 1981; Kusumi et al., 1982a; Subczynski & Hyde, 1983; Subczynski et al., 1987, 1989, 1990). The major objectives of these studies are (1) to understand the transport mechanism of small molecules in the membrane and (2) to study the interaction between the phosphatidylcholine (PC) and cholesterol by using small molecules as a probe. We paid special attention to the differences in lipid interaction and organization between saturated PC–cholesterol and unsaturated PC–cholesterol membranes. In order to give a clear presentation, our previous results and models on PC–cholesterol interaction and microimmiscibility in the membrane are summarized in the text section.

Our method to study transport of small molecules is based on the measurement of the bimolecular collision rate between these paramagnetic molecules (fast relaxing species) and the nitroxide spin label (a slow relaxing species) in the membrane by observing the spin-lattice relaxation times (T_1's) of the spin labels. The collision rate is proportional to the product of the local concentration and the local diffusion coefficient, and thereby to the transport coefficient, of the paramagnetic molecules at a specific place in the membrane (see Experimental Procedures).

In the course of this series of studies, a preliminary observation of anomalous behaviors of oxygen transport in L-α-dioleoyl-PC (DOPC, an unsaturated PC)–cholesterol membranes was made. Oxygen transport in the central part of the membrane was *increased* by incorporation of cholesterol in DOPC membranes in the liquid-crystalline state (Subczynski et al., 1989). One of the thrusts of the present work is, thereby, to elucidate the relationships between oxygen transport and lipid organization in the membrane in order to understand the molecular mechanism of membrane transport and diffusion.

We will advance the idea of vacant pockets created both intramolecularly and intermolecularly in the membrane as an important structural factor for oxygen transport in the membrane. Oxygen molecules may hop from one pocket to the adjacent pocket in the membrane or may be carried along in the pocket as the pocket migrates. These vacant pockets would be formed by dynamic gauche–trans isomerism of alkyl chains and the conformational mismatch between adjacent lipid molecules, cholesterol, and unsaturated PC in particular.

We will pay special attention to (1) the influence of the double bond in PC alkyl chains on oxygen transport in membranes and to (2) the conformational mismatch between cholesterol and unsaturated PC alkyl chains as it relates to oxygen transport in the membrane. Because introduction of alkyl chain unsaturation and variation of the cholesterol mole fraction induce large changes in conformation of the adjacent lipids, lipid–lipid interaction, and lipid-domain organization in the membrane (see the following section for a review), by studying the influences of these changes on oxygen transport, we would gain important insight into the mechanism of oxygen
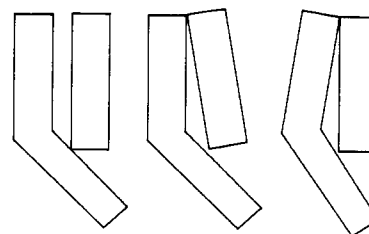

FIGURE 1: Schematical drawings showing that nonconformability of the rigid ring structure of cholesterol (rectangles) and the rigid bend at the C9–C10 cis double bond in an unsaturated alkyl chain (bent rods) induces vacant pockets (packing defects) in the membrane. Three possible configurations are indicated. In neither case is good packing possible.

transport in the membrane. The results on oxygen transport are compared with the transport and diffusion data for phospholipids and CuKTSM$_2$ (Kusumi et al., 1986; Subczynski et al., 1990). On the basis of these observations, we propose a molecular mechanism of oxygen transport in the membrane and also a mechanism by which alkyl chain unsaturation and cholesterol affect the oxygen transport in the membrane.

Summary of the Previous Studies on the Effect of Cholesterol Incorporation in PC Membranes. Previously, we have studied PC–cholesterol interaction in various unsaturated PC and unsaturated PC membranes (Kusumi et al., 1983, 1986; Subczynski & Kusumi, 1986; Merkle et al., 1987; Kusumi & Pasenkiewicz-Gierula, 1988; Pasenkiewicz-Gierula et al., 1990; Subczynski et al., 1990). These studies as well as those by Shin and Freed (1989a,b) and Shin et al. (1990) indicated that PC–cholesterol interaction in the membrane is quite different between saturated and unsaturated (C9–C10-*cis*) PC membranes: cis-unsaturated PC is less miscible with cholesterol at physiological temperatures than saturated PC, while the major effect of cholesterol on saturated PC is to mix at certain ratios and to enhance the trans configuration of the saturated chain (Vist & Davis, 1990).

We have proposed the following model for the molecular interaction of cholesterol and PC to explain a variety of cholesterol effects (CE) in PC–cholesterol membranes.

(CE1) Intercalation of cholesterol promotes trans configuration (extended structure) of single bonds in saturated PC membranes due to its rigid plate-like ring structure [i.e., the so-called "ordering effect of cholesterol" (Presti, 1985; Kusumi et al., 1986)].

(CE2) The rigid tetracyclic ring structure of cholesterol and the rigid bend at the double bond in unsaturated PC alkyl chains do not conform to each other when they are in direct contact in the membrane (Pasenkiewicz-Gierula et al., 1990; Subczynski et al., 1990). This structural nonconformability is most significant with a cis double bond in the alkyl chain. The nonconformability between the rigid ring structure of cholesterol and the rigid bend at the C9–C10 cis double bond in the unsaturated alkyl chain is the key feature of unsaturated PC–cholesterol interaction [see Figure 1; the readers are urged to refer to Figure 8 in Pasenkiewicz-Gierula et al. (1990)].

(CE3) The mismatch in length[3] between PC alkyl chains

---

[3] The match in hydrophobic lengths between phospholipid alkyl chains and a membrane protein (rhodopsin) was found to be important in determining the equilibrium between the association states of the protein in the membrane. Rhodopsin stays as monomers in lipid-rich dipalmitoyl-PC membranes, and dimeric (or oligomeric) association of rhodopsin becomes prevalent in dilauroyl-PC (which has shorter alkyl chains) and distearoyl-PC (which has longer alkyl chains) membranes. This tendency is enhanced in protein-rich membranes. It is concluded that, in the native rod outer segment membranes, monomeric and dimeric rhodopsin molecules are in equilibrium (Kusumi & Hyde, 1982).

and cholesterol (the bulky ring structure, in particular) creates free volume in the central part of the bilayer[4] (Subczynski et al., 1990). This effect is enhanced in the presence of the double bond in the alkyl chain because of the structural nonconformability between cholesterol and unsaturated PC (CE2).

(CE4) Intercalation of cholesterol increases the space between lipid molecules in the headgroup region, which water molecules enter.

As a result of the structural nonconformability of cis-unsaturated PC and cholesterol (CE2), the following secondary effects of cholesterol are induced.

(CE2-1) Cholesterol molecules tend to be segregated out of the unsaturated PC domain and form cholesterol-rich or cholesterol oligomeric domains, which are small (several lipids) and/or of short lifetime (10^{-9}–10^{-7} s) (Pasenkiewicz-Gierula et al., 1990; Subczynski et al., 1990).

(CE2-2) More and larger vacant pockets are created in unsaturated PC–cholesterol membranes than in unsaturated PC membranes without cholesterol (or in saturated PC membranes with and without cholesterol), as is shown in Figure 1.

(CE2-3) The ordering effect of cholesterol is weaker in unsaturated PC membranes than that in saturated PC membranes due to CE2-1 and CE2-2 (Subczynski et al., 1990).

One of the major objectives in the present work is to study CE2-2 in more detail in terms of oxygen transport in the membrane and to elucidate the mechanism of oxygen transport in phospholipid–cholesterol membranes.

EXPERIMENTAL PROCEDURES

Materials. All PCs were obtained from Sigma, cholesterol (crystallized) was from Boehringer Mannheim, 5- and 16-SASL and 14-doxyleicosanoic acid spin label (14-EASL) were from Molecular Probes (Junction City, OR), and 1-oxyl-4-oxo-2,2,6,6-tetramethyl[1-^{15}N]piperidine-d_{16} (*d*-tempone) was from Merck. T-PC was a generous gift from Dr. S. Ohnishi (Kyoto University, Kyoto, Japan). The buffer used was 0.1 M sodium borate at pH 9.5. To ensure that all carboxyl groups of stearic acid spin labels (SASL) were ionized in PC membranes, a rather high pH was chosen (Sanson et al., 1976; Egret-Charlier et al., 1978; Kusumi et al., 1982a,b, 1986). The structures of PC membranes are not altered at this pH (Träuble & Eibl, 1974; Kusumi et al., 1982a, 1986).

Membrane Preparation and ESR Measurement. The membranes used in this work were multilamellar dispersions of lipids containing 1 mol % of spin label and were prepared as described (Kusumi et al., 1982a, 1986). The lipid dispersion (10^{-5} mol of total lipid/1 mL) was centrifuged briefly, and the loose pellet ($\approx$20% lipid w/w) was used for ESR measurement. Dilution of the pellet did not induce any detectable changes in the membrane structure (Kusumi et al., 1986). The sample was placed in a capillary (i.d. = 0.5 mm) made of a gas-permeable polymer called TPX (Hyde & Subczynski, 1989). The concentration of oxygen in the sample was controlled by equilibrating the sample with the same gas that was used for temperature control, i.e., a controlled mixture of nitrogen and dry air adjusted with flowmeters (Matheson Gas Products; model 7631H-604) (Kusumi et al., 1982a; Hyde & Subczynski, 1989). T_1's of the spin labels were measured at X-band by using the long-pulse saturation–recovery technique (Kusumi et al., 1982a; Subczynski et al., 1989, 1990). With long and intense microwave pulses, the spin system approaches a steady state at which the population of spins at each energy level tends to be equalized. After the saturating pulse is turned off, the recovery of the spin system to Boltzmann equilibrium is observed with a weak observing power. In general, the nitrogen nuclear spin-lattice relaxation time is much shorter than the electron spin-lattice relaxation time for spin labels in membranes (Yin et al., 1987; Yin & Hyde, 1987), and single-exponential decays were found. The duration of the saturating pulse is then not critical. However, if the electron spin-lattice relaxation becomes sufficiently short by introduction of high concentrations of molecular oxygen, multiple–exponential signals are expected, and the long-pulse techniques should be used. The saturation–recovery spectrometer is based on the design of Huisjen and Hyde (1974) and is interfaced with a loop-gap resonator. A field-effect transistor microwave amplifier has been recently introduced. Typically, 2 × 10^7 accumulations of the decay signal were carried out with 128–512 data points on each decay. Accumulation time was typically 5 min. The apparatus used here was described previously (Yin et al., 1987; Subczynski et al., 1990).

Calculation of the Oxygen Transport Parameter and Oxygen Permeability Across the Membrane. Bimolecular collision of molecular oxygen (a fast relaxing species) and the nitroxide (a slow relaxing species) induces spin exchange, which leads to a faster effective spin-lattice relaxation of the nitroxide. The bimolecular collision rate was evaluated by measuring T_1's of the nitroxide as a function of the partial pressure of oxygen using the long-pulse saturation–recovery ESR technique. An oxygen transport parameter $W(x)$ was introduced as a convenient quantitative measure of the collision rate between the spin label and molecular oxygen (Kusumi et al., 1982a):

$$W(x) = T_1^{-1}(\text{air}, x) - T_1^{-1}(N_2, x) \qquad (1)$$

Note that $W(x)$ is normalized to the sample equilibrated with the atmospheric air. $W(x)$ is proportional to the product of the local concentration $C(x)$ and the local translational diffusion coefficient $D(x)$ of oxygen (thus called a transport parameter) at a "depth" x in the membrane (which is in equilibrium with the atmospheric air):

$$W(x) = AD(x)C(x) \qquad (2)$$

$$A = 8\pi p r_0 \qquad (3)$$

where r_0 is the interaction distance between oxygen and the nitroxide radical spin labels ($\approx$4.5 Å) and p is the probability that an observable event occurs when a collision does occur (Subczynski & Hyde, 1984; Hyde & Subczynski, 1984). A is remarkably independent of the solvent viscosity, hydrophobicity, temperature, and spin label species (Subczynski & Hyde, 1981, 1984; Hyde & Subczynski, 1984, 1989). It was found that the oxygen transport parameter is a useful monitor of membrane fluidity that reports on translational diffusion of small molecules in the membrane. In addition, the chemical reaction rate of oxygen in the membrane is proportional to $W(x)$ if chemical reaction does occur in the membrane. The membrane profiles of $W(x)$ were constructed on the basis of the measurements with T-PC, 5-SASL, and 16-SASL.

---

[4] The cholesterol molecule contains three well-distinguished regions: the small polar hydroxyl group, the rigid plate-like steroid ring, and the isooctyl chain tail. When cholesterol intercalates into the membrane, its polar hydroxyl group is positioned near the middle of the glycerol backbone region of the PC molecule (Franks & Lieb, 1979). The rigid steroid ring reaches to a depth of about the 7th to 10th carbon (McIntosh, 1978). The isooctyl tail of cholesterol reaches to the 12th to 15th carbons. The presence of cholesterol increases the free space in the central part of the bilayer because the cross section of the steroid ring is larger than that of its hydrocarbon tail (Subczynski et al., 1990).

Table I: $T_1(\mu s)$ for T-PC, 5-SASL, and 16-SASL in a Variety of PC–Cholesterol Membranes at 45 °C[a]

spin label	cholesterol mole fraction (%)	DLPC	DMPC	DPPC	DSPC[b]	DEPC	DOPC	EYPC
T-PC	0	2.62	2.65	2.65	2.23	2.48	2.30	2.28
	30	ND[c]	2.65	ND	2.15	ND	2.30	2.33
	50	1.97	2.00	2.00	1.87	2.07	2.00	2.05
5-SASL	0	3.19	3.16	3.45	2.95	3.15	3.30	3.54
	30	ND	3.50	ND	2.95	ND	3.50	3.78
	50	3.41	3.87	3.82	3.15	3.35	3.70	3.90
16-SASL	0	2.03[d]	1.76	1.77	1.60	1.70	1.75	1.83
	30	ND	1.45	ND	1.30	ND	1.69	1.71
	50	2.03[d]	1.36	1.26	1.25	1.53	1.64	1.62

[a] The accuracy is within 5%. With an increase of the cholesterol concentration, T_1 for T-PC and 16-SASL decreases while T_1 for 5-SASL increases. [b] Measured at 56.5 °C. [c] ND = not determined. [d] The spin label used was 14-EASL.

Oxygen permeability across the membrane was calculated on the basis of the membrane profile of $W(x)$ by using (Subczynski et al., 1989)

$$P_M = \frac{1}{AC_W(air)} \left[\int_0^{\delta_M} \frac{dx}{W(x)} \right]^{-1} \quad (4)$$

where δ_M is the thickness of the bilayer membrane and $C_W(air)$ is the oxygen concentration in water that is in equilibrium with atmospheric air under the given temperature. The oxygen permeability across the water layer that has the same thickness as the membrane was calculated by

$$P_W(\text{pulse ESR}) = \frac{1}{AC_W(air)} \frac{W(d\text{-tempone})}{\delta_M} \quad (5)$$

$$P_W(\text{bulk water}) = D_O(\text{bulk water})/\delta_M \quad (6)$$

where $W(d\text{-tempone})$ is the oxygen transport parameter in water as measured with d-tempone by using the pulse ESR technique and $D_O(\text{bulk water})$ is the diffusion coefficient of molecular oxygen in the bulk water [from the data of St.-Denis and Fell (1971)].

Results and Discussion

The membranes examined in this work include those made of egg-yolk PC [EYPC, mixed PC containing both saturated and unsaturated alkyl chains, approximately 70% is 1-palmitoyl-2-oleoyl-PC (Seelig & Waespe-Šarčević, 1978)], DOPC (18 carbons per alkyl chain, 9–10-cis unsaturated), L-α-dielaidoyl-PC (DEPC, 18 carbons, 9–10-trans unsaturated), L-α-distearoyl-PC (DSPC, 18 carbons, saturated), L-α-dilauroyl-PC (DLPC, 12 carbons, saturated), L-α-dimyristoyl-PC (DMPC, 14 carbons, saturated), and L-α-dipalmitoyl-PC (DPPC, 16 carbons, saturated) with 0–50 mol % of cholesterol.

All measurements of T_1 were made on the central line of the ESR spectrum between 0 and 56.5 °C. Typical saturation recovery curves are shown in Figure 2 of Subczynski et al. (1990). The signal-to-noise ratio was high enough to allow us to obtain T_1 of spin labels within an accuracy better than 5%.

Effect of Cholesterol on T_1 in the Absence of Molecular Oxygen. First, we discuss the effect of cholesterol incorporation of T_1's in the absence of oxygen molecules. T_1 data are summarized in Table I. In the absence of oxygen, incorporation of cholesterol *decreases* T_1 of T-PC and 16-SASL, while it slightly increases T_1 of 5-SASL in all membranes studied here.

Since the dominant T_1 mechanism for the nitroxide radicals has not been known, the quantitative explanation for our observation described above is not possible at this point. The conventional ESR spectroscopy of spin-labeled EYPC–

cholesterol membranes indicated that the presence of cholesterol induces a small increase in the order parameter of 5-SASL and 16-SASL and an increase in mobility (although in complicated ways) of T-PC. Shin and Freed (1989a) reported a cholesterol-induced increase in both order parameter and wobbling rotational diffusion coefficient (R_{perp}) of 16-doxyl-PC spin label in 1-palmitoyl-2-oleoyl-PC membranes. The cholesterol-induced enhancement of motion of the choline group in the PC headgroup in DPPC membranes was shown by Oldfield et al. (1978). Taken together, we think that the above results induced by cholesterol insertion reflect the enhancement of one or more of the complex motional modes of the nitroxide group in T-PC and 16-SASL, which is induced by the formation of space between lipid molecules in the headgroup region (CE4) and in the central part of the lipid bilayer (CE3) in the presence of cholesterol. The cholesterol-induced increase of T_1 in 5-SASL regions is also probably related to 5-SASL motion. Cholesterol decreases the reorientation rate of 5-SASL and increases alkyl chain order (although this effect is small in unsaturated PC membranes).

Saturation–Recovery Measurement of the Oxygen Transport Parameter. In Figure 2, T_1^{-1} in EYPC–cholesterol membranes obtained for air- or nitrogen-equilibrated samples is plotted as a function of inverse temperature. In the presence of oxygen, T_1 decreases substantially due to an additional relaxation pathway provided by the collision with molecular oxygen.

$W(x)$ values for EYPC–cholesterol membranes calculated according to eq 1 on the basis of the data in Figure 2 are displayed in Figure 3. The presence of cholesterol decreases $W(x)$ in and near the headgroup region (as detected with T-PC and 5-SASL, Figure 3A,B). In contrast, inclusion of cholesterol *increases* $W(x)$ in the central part of the bilayer as detected with 16-SASL (Figure 3C). This cholesterol-induced increase of $W(16\text{-SASL})$ contradicts with the general idea of the "rigidifying" effect of cholesterol in the fluid phase, i.e., decreasing the membrane fluidity, and will be discussed further later [for reviews, see Demel and de Kruyff (1976), Presti (1985), and Yeagle (1985, 1988)].

Effect of Unsaturation on $W(x)$. In this section, we will concentrate on the difference in $W(x)$ between saturated and unsaturated PC membranes *in the absence of cholesterol.* In Table II, $W(x)$ values in EYPC, DOPC, DEPC, DPPC, and DMPC membranes without cholesterol in the liquid-crystalline phase are summarized. At all membrane locations studied here, $W(x)$ is *smaller* in unsaturated PC membranes with *either cis or trans* double bond (EYPC, DOPC, DEPC) than in saturated PC membranes (DMPC and DPPC). This observation contradicts with the general view of the effect of introduction of unsaturation into the alkyl chain on membrane
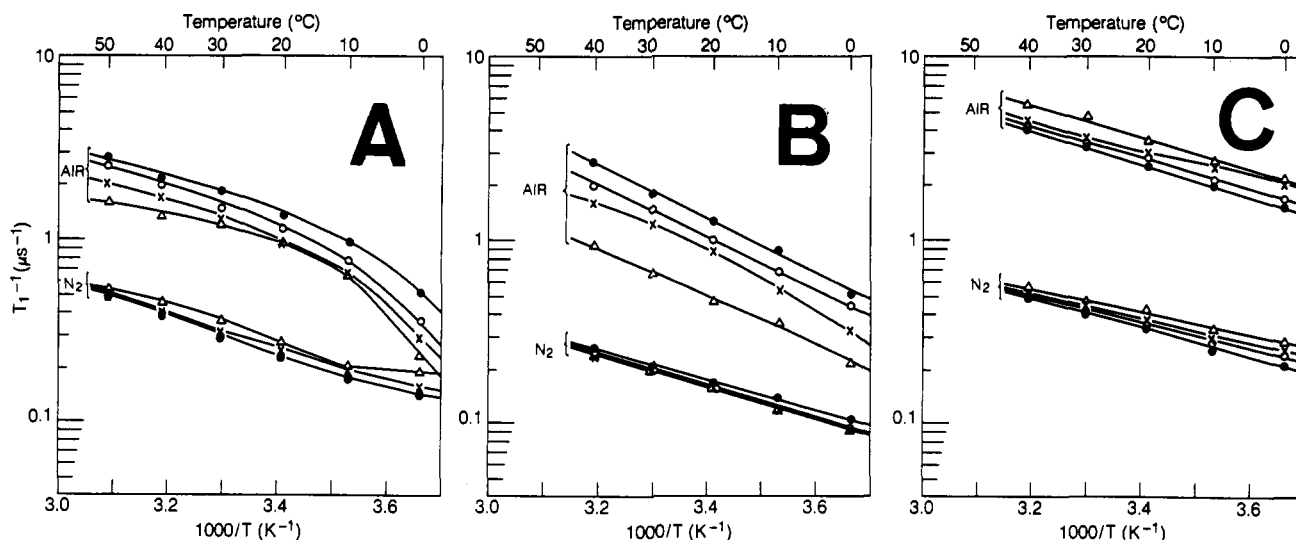
FIGURE 2: T_1^{-1} as a function of reciprocal temperature for T-PC (A), 5-SASL (B), and 16-SASL (C) in EYPC–cholesterol membranes equilibrated either with air or nitrogen gas. Actual measurements with oxygen were carried out for samples equilibrated with a gas mixture containing 33% or 50% air and extrapolation was made to 100% air on the basis of the linear dependence of T_1^{-1} as a function of oxygen concentration in the equilibrating gas (Kusumi et al., 1982a). Symbols: 0 ($\bullet$), 15 (O), 27.5 ($\times$), and 50 ($\triangle$) mol % cholesterol.
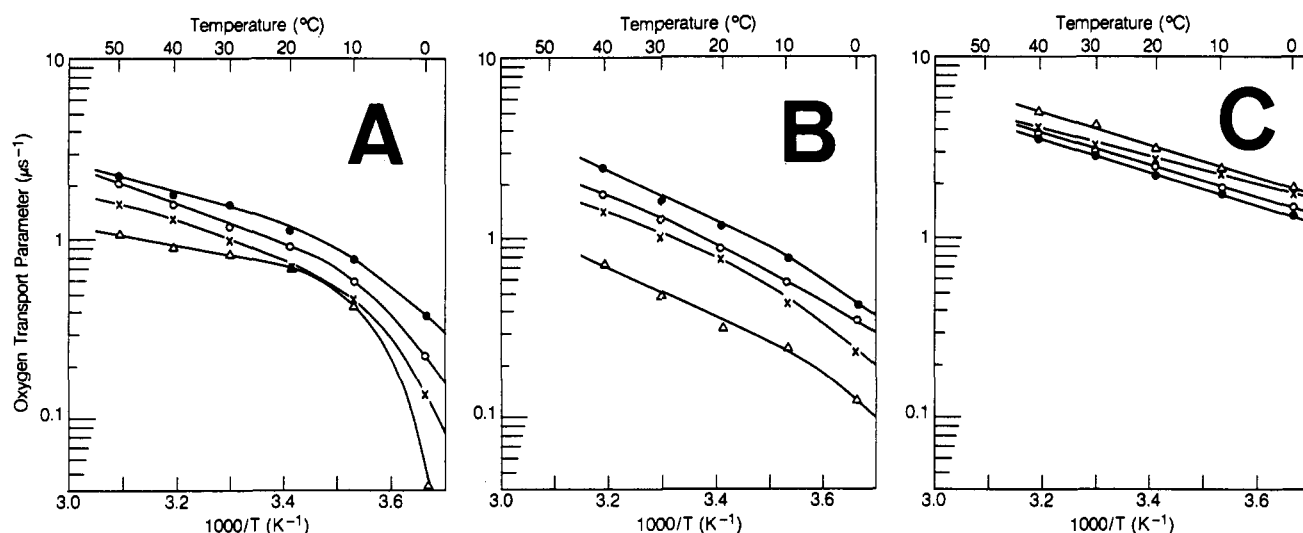

FIGURE 3: $W(x)$ as a function of reciprocal temperature for T-PC (A), 5-SASL (B), and 16-SASL (C) in EYPC–cholesterol membranes. Symbols: 0 ($\bullet$), 15 (O), 27.5 ($\times$), and 50 ($\triangle$) mol % cholesterol.

Table II: Effect of the Double Bond in the Alkyl Chain on the Oxygen Transport Parameter[a]

spin label	EYPC	DOPC	DEPC	DPPC	DMPC
T-PC	2.0	2.0	2.1	2.6	2.8
5-SASL	2.6	2.1	2.1	2.8	3.0
16-SASL	3.8	3.6	3.4	4.4	4.7

[a] $W(x)$ (± 0.3 μs^{-1}) values were estimated in various PC membranes in the fluid phase in the absence of cholesterol at 45 °C.

fluidity, i.e., that unsaturation would increase the fluidity and thus $W(x)$ (Jain & Wagner, 1980).

We think that the key feature of oxygen transport in the membrane is the small size of oxygen. Since molecular oxygen is small, its diffusion mechanism in the membrane must be quite different from that of lipids and other molecules studied previously. We suggest that oxygen transport in the membrane is closely related to creation and movements of small but many vacant pockets due to rapid gauche–trans isomerization of alkyl chains and conformational mismatch between lipid molecules.

The presence of either a cis or trans double bond in the alkyl chain would reduce the dynamics of the chain around the

double bonds. The data reported by Seelig and Waespe-Šarčević (1978) are consistent with this model. In addition, in the unsaturated PC membranes studied above, the double bonds are concentrated in the region of C9–C10, which would produce two belted regions in the membrane in which alkyl chain dynamics is rather reduced. These two effects, coupled together, would decrease the oxygen transport in the membrane (refer to Figure 8).

Träuble (1971) and Pace and Chan (1982) advanced the argument on the relationships between the diffusion of small molecules in the membrane and kink migration and/or kink formation due to the alkyl chian isomerization. The inhibition of these dynamic kink processes as the result of the presence of double bonds in the alkyl chains would decrease the oxygen transport parameter. In particular, the kink migration would be strongly suppressed by the double bonds in the chain. The idea of vacant pockets in the membrane presented here is similar to these kink models, but the vacant pockets cover the wider ranges of packing defects in the membrane, and, as will be shown later in this report, vacant pockets formed by a variety of mechanisms contribute to the oxygen transport in
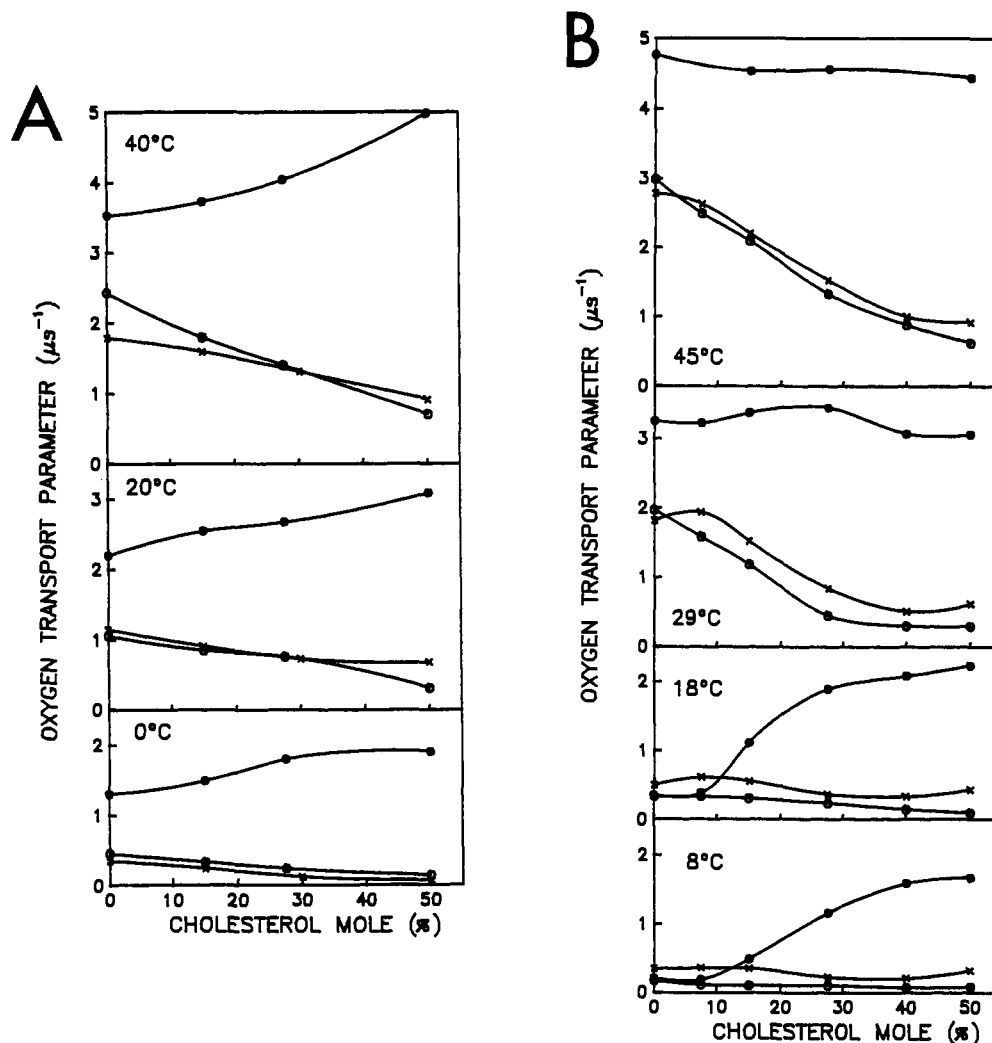
FIGURE 4: $W(x)$ plotted as a function of cholesterol mole fraction in (A) EYPC–cholesterol membranes and (B) DMPC–cholesterol membranes. Symbols: (×) T-PC, (○) 5-SASL, and (●) 16-SASL.

the membrane. However, since we do not possess sufficient data on the kink conformation of the alkyl chains in the membrane, we would refrain from further discussion on the relationships between kink conformation and diffusion of small molecules.

Cholesterol Effect on $W(x)$ in EYPC and DMPC Membranes. The dependence of $W(x)$ on cholesterol mole fraction in EYPC-cholesterol membranes is shown in Figure 4A. As described above, $W(x)$ increases in 16-SASL region and decreases in T-PC and 5-SASL regions as the cholesterol mole fraction is increased from 0 to 50 mol % in EYPC membranes.

$W(x)$ vs cholesterol mole fraction in DMPC-cholesterol membranes is shown in Figure 4B. In the liquid-crystalline phase of DMPC–cholesterol membranes at 45 and 29 °C, an increase in cholesterol mole fraction induces a large decrease in $W(x)$ in T-PC and 5-SASL regions but causes only slight changes in $W(x)$ in 16-SASL regions. Below the phase-transition temperature of DMPC membranes (at 18 and 8 °C), the cholesterol effect is small in T-PC and 5-SASL regions while it causes a large *increase* in the 16-SASL regions. This increase starts above 10 mol % of cholesterol.

The most remarkable feature in Figure 4A,B is the cholesterol effect in the central part of the bilayer in the liquid-crystalline phase, i.e., $W(16\text{-SASL})$ increases with an increase of the cholesterol mole fraction in EYPC–cholesterol membranes, while it shows little changes in DMPC–cholesterol membranes. These cholesterol effects may be explained by

(I) the mismatch in length between PC alkyl chains and the bulky ring structure of cholesterol (CE3) and/or (II) the structural nonconformability of cholesterol and unsaturated alkyl chains [CE2-2, Figures 1 and 8, Pasenkiewicz-Gierula et al. (1990), and Subczynski et al. (1990)]. These effects would work cooperatively. Nevertheless, we will discuss further on which effect contributes more to the cholesterol-induced increase of $W(16\text{-SASL})$ in EYPC membranes after we present Figure 6.

In our previous reports (Pasenkiewicz-Gierula et al., 1990; Subczynski et al., 1990), a model (CE2-1) was proposed in which the fluid-phase immiscibility is prevalent in cis-unsaturated PC–cholesterol membranes but where cholesterol-rich (cholesterol-oligomeric) domains are small (several lipids) and/or of short lifetime (10^{-9}–10^{-7} s). It was also concluded by Shin and Freed (1989a,b) and Shin et al. (1990) that acyl chain unsaturation leads to poorer mixing of cholesterol in the PC membranes in the liquid-crystalline phase. The present measurement of oxygen transport in membranes did not detect any specific indications of the microimmiscibility probably because the present method is not sensitive enough to detect the existence of the cholesterol-rich (or cholesterol-oligomeric) domains of the size and the lifetime indicated above.

In the case of DMPC–cholesterol membranes, because the alkyl chains of DMPC are shorter and saturated, the mismatch in length is smaller (I above) and the conformability of the cholesterol ring structure and the alkyl chain is better (II

Table III: Activation Energy for the Translational Diffusion of Molecular Oxygen in EYPC–Cholesterol and DMPC–Cholesterol Membranes

host lipid	cholesterol mole fraction (%)	act. energy (kcal/mol)			temp range (°C)
		T-PC	5-SASL	16-SASL	
DMPC	0	5.6	4.3	3.7	30–45
	27.5	7.1	13.0	3.7	30–45
	50	5.3	9.5	3.7	30–45
EYPC	0	3.7[a]	6.5	4.2	10–40
	27.5	5.0[a,b]	6.2	4.1	10–40
	50	2.6[a]	6.3	4.2	10–40

[a] Evaluated between 20 and 50 °C. [b] The cholesterol mole fraction for this measurement is 30%.

above). The cholesterol effect of creation of the vacant pockets in the central part of the bilayer (this effect is rather small anyway in DMPC–cholesterol membranes) and the ordering effect of cholesterol on the myristoyl chain would cancel out each other, inducing little changes in W(16-SASL) in DMPC–cholesterol membranes.

W(T-PC) decreases with an increase of cholesterol mole fraction both in EYPC and DMPC membranes as shown in Figure 4. Previously, we have made two observations on cholesterol effects on T-PC. (1) The water accessibility to the nitroxide group of T-PC increases with an increase of cholesterol content in the membrane (Kusumi et al., 1986; Kusumi & Pasenkiewicz-Gierula, 1988). (2) The reorientation rate of the nitroxide of T-PC increases in complex ways with an increase of the cholesterol content in the membrane (Subczynski et al., 1989). These observations were explained by formation of free space in the headgroup region due to separation of PC headgroups by intercalation of cholesterol, into which water molecules partition (CE4). The large cholesterol-induced decreases in W(T-PC) shown in Figure 4A,B are apparently contradictory to this explanation. We suggest that oxygen diffusion from the membrane side may be reduced in the presence of cholesterol. It is possible that T-PC may be monitoring not only the headgroup region but also the hydrophobic region near the membrane surface where the oxygen transport is reduced by the presence of cholesterol. However, we do not think this likely because the collision of T-PC with 5-, 12-, and 16-SASL cannot be detected by electron–electron double resonance ESR spectrometry [the collision rate between 5- and 16-SASL is as high as 10^5–10^6 s^{-1} (Feix et al., 1987; J. B. Feix and J. S. Hyde, unpublished observation)].

Activation Energy for Translational Diffusion of Oxygen in EYPC–Cholesterol and DMPC–Cholesterol Membranes. The oxygen transport parameter plotted in Figure 3 shows linear dependence on reciprocal temperature above 0, 10, 20 °C for 16-SASL, 5-SASL, and T-PC, respectively. Since the overall oxygen concentration in the membrane is practically independent of temperature above the phase-transition temperature (Subczynski & Hyde, 1983; Subczynski, 1984; Smotkin et al., 1991) and the shape of the membrane profile of $W(x)$ varies little with temperature in the liquid-crystalline phase, the temperature-dependent changes of $W(x)$ can be attributed to those of the diffusion coefficient of molecular oxygen in the membrane. Thus from the slope of the plots of $W(x)$ vs T^{-1}, the activation energy for oxygen diffusion in the membrane was evaluated and is listed in Table III. The activation energy for DMPC–cholesterol membranes is also summarized, which was calculated on the basis of our previous

data between 30 and 45 °C (Subczynski et al., 1989).

In the absence of cholesterol, the activation energy for the translational diffusion of molecular oxygen (3.7–6.5 kcal/mol) is substantially smaller than that of larger membrane-soluble molecules; 8–11 kcal/mol for a square-planar copper complex CuKTSM$_2$ (MW = 393.5, 8 × 8 Å square-plane) and 6.5–15 kcal/mol for phospholipids (MW = 650–1000). This result suggests that the mechanism of translational diffusion of molecular oxygen is quite different from that of larger molecules such as CuKTSM$_2$ and phospholipids. As stated in the introductory section, Träuble (1971) and Pace and Chan (1982) estimated the activation energy to be 4.8 kcal/mol for kink migration (with which oxygen molecules can be carried along) and 3.1 kcal/mol for C–C bond rotation to produce the kink structure in the alkyl chain, respectively. The activation energy obtained here for the translational diffusion of oxygen in the 5-SASL region, at which these estimates are applicable, is 4.3 kcal/mol, quite close to these theoretical evaluations.

The activation energy for translational diffusion of molecular oxygen in DMPC and EYPC membranes is quite different. The activation energy in the 5-SASL region in EYPC membranes is 50% larger than that in DMPC membranes. This result is consistent with the vacant pocket model described above because the presence of the double bond in EYPC membranes would decrease the alkyl chain dynamics, resulting in larger resistance to oxygen diffusion in this region. In the T-PC headgroup region, the activation energy is smaller in EYPC membranes than in DMPC membranes. This may be related to the larger surface area per molecule in EYPC membranes (72–74 Å^2/EYPC; Small, 1967; Levine & Wilkins, 1971; Tinker et al., 1976; Lis et al., 1982) than in DMPC membranes (61–66 Å^2/DMPC; Curatro et al., 1977; Janiak et al., 1979; Lis et al., 1982; Cornell & Separovic, 1983). The more space in the headgroup region would reduce the activation energy.

In the presence of cholesterol, the major difference in the activation energy is a 3-fold increase detected with 5-SASL in DMPC–30 mol % cholesterol membranes. If we assume that the oxygen diffusion in the membrane is strongly dependent on the rate of gauche–trans isomerization of the alkyl chain or the number of gauche conformation in the alkyl chain, this result is consistent with the observation in which the rigid steroid ring structure of cholesterol enhances the trans conformation adjacent to the ring (Presti & Chan, 1982; Presti et al., 1982; Kusumi et al., 1986).

The activation energies for W(5-SASL) and W(T-PC) in 30 mol % cholesterol–DMPC membranes are larger than those in either 0 or 50 mol % cholesterol–DMPC membranes. These results are consistent with our previous observation in which the activation energy for the wobbling rotational diffusion of cholesterol-analogue spin label in DPPC–cholesterol membranes is largest at 15–30 mol % cholesterol (Pasenkiewicz-Gierula et al., 1990). In the phase diagram of DMPC–cholesterol membranes (Recktenwald & McConnell, 1981; Kusumi et al., 1986; Ipsen et al., 1987; Pasenkiewicz et al., 1990), the present measurements at 0 and 30 mol % cholesterol are mostly in the region I, while those at 50 mol % cholesterol are in the region III.

Cholesterol Effect on $W(x)$ in DOPC–Cholesterol Membranes. In order to further examine the influence of alkyl chain unsaturation on the cholesterol effect on $W(x)$, we studied $W(x)$ in DOPC–cholesterol membranes. Since DOPC has a single cis double bond at C9–C10 position in each alkyl chain, the effect of a cis double bond can be specifically examined. T_1 and $W(x)$ in DOPC–cholesterol membranes change as a
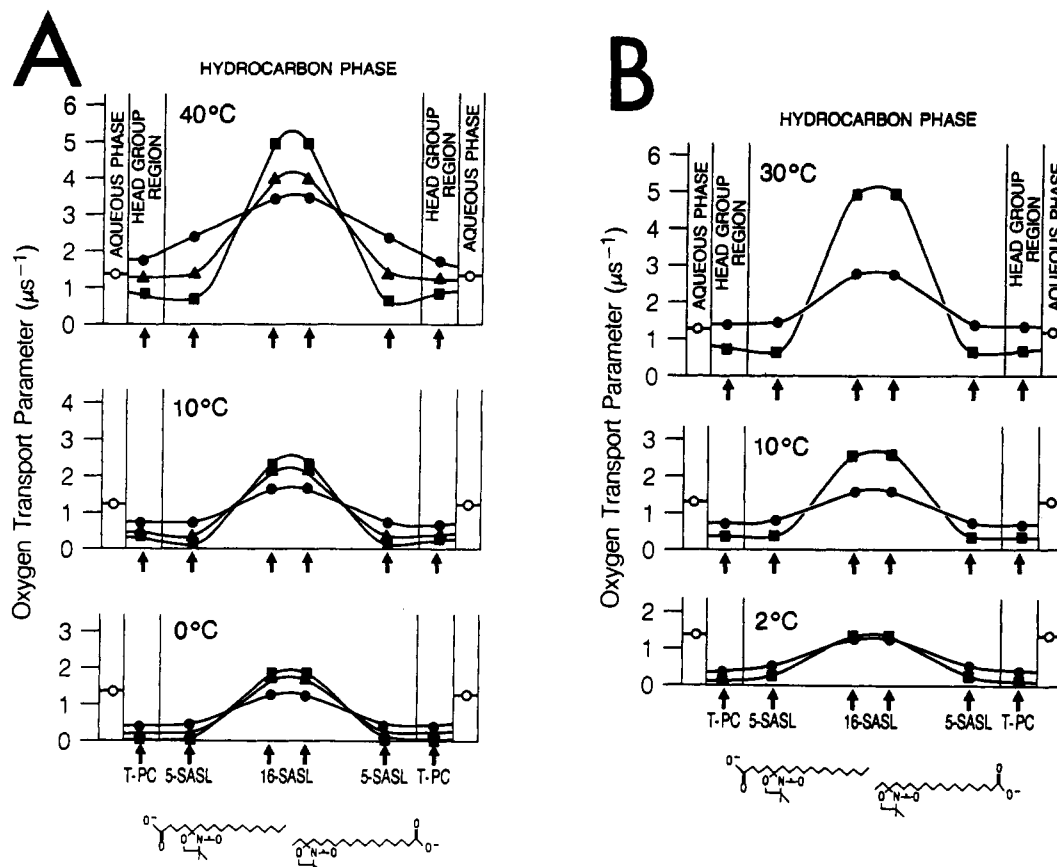
FIGURE 5: Effect of cholesterol on $W(x)$ profiles across EYPC (A) and DOPC (B) membranes evaluated with T-PC, 5-SASL, and 16-SASL. $W(x)$ in the aqueous phase was obtained by using d-tempone. Approximate locations of the nitroxide moieties of spin labels are indicated by arrows and schematic drawings. Symbols: 0 (●), 27.5 (▲), and 50 (■) mol % cholesterol.

function of cholesterol and temperature in a qualitatively similar way with those in EYPC–cholesterol membranes (the data were omitted to save space and are available on request). In particular, the presence of cholesterol decreases $W(x)$ in and near the headgroup region (as detected with T-PC and 5-SASL), while it *increases* $W(x)$ in the central part of the bilayer (as detected with 16-SASL).

Since the locations of the spin labels in the membrane are quite well defined, the membrane profiles of $W(x)$ can be constructed. $W(x)$ profiles for DOPC–cholesterol membranes are shown in Figure 5 together with those for EYPC–cholesterol membranes. The membrane profiles of $W(x)$ for DMPC–cholesterol membranes have already been published (Subczynski et al., 1989). The oxygen transport parameter in the aqueous phase obtained with d-tempone is also shown for comparison. Notice that the temperature dependence of oxygen transport parameter in the aqueous phase is almost absent due to the opposite effect of temperature on oxygen solubility and translational diffusion. The most striking feature in these figures is again the induction of large increases of $W(x)$ in the central part of the bilayer by incorporation of cholesterol in the membrane.

Differential Effect of Cholesterol on $W(x)$ in Saturated and Unsaturated PC Membranes. The effects of cholesterol intercalation on $W(x)$ in various membranes are summarized in Figure 6, in which the ratio of W(50 mol % cholesterol)/ W(no cholesterol) is plotted for three spin labels (T-PC, 5-SASL, and 16-SASL) in seven kinds of PC membranes (DLPC, DMPC, DPPC, DSPC, DEPC, DOPC, and EYPC). The cholesterol effects are quite similar in all membranes in and near the headgroup regions (as detected with T-PC and 5-SASL), decreasing $W(x)$ in these regions.
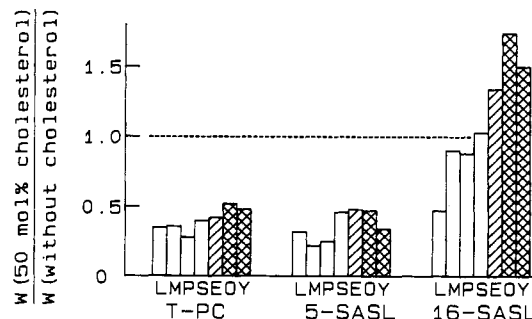

FIGURE 6: Effect of 50 mol % cholesterol on $W(x)$. The ratio of $W(x)$ values with and without 50 mol % cholesterol is measured at 45 °C in various PC ± cholesterol membranes. Symbols: L, DLPC; M, DMPC; P, DPPC; S, DSPC; E, DEPC; O, DOPC; and Y, EYPC; open bars, saturated chain; hatched bars, trans unsaturation; cross-hatched bars, cis unsaturation. In order to evaluate $W(x)$ in the central region of the DLPC ± cholesterol membranes, 14-EASL was used instead of 16-SASL. For DSPC ± cholesterol membranes, the measurements were carried out at 56.5 °C.

The major differences among various membranes take place in the central region of the membrane as detected with 16-SASL: (1) The cholesterol effect is small (the ratio is close to 1) in saturated PC membranes (DMPC, DPPC, and DSPC) except in DLPC membranes. (2) In DLPC membranes, 50 mol % cholesterol decreases W(16-SASL) by a factor of 2. (3) In unsaturated PC membranes, the ratio is larger than 1, i.e., cholesterol increases W(16-SASL) in both cis and trans unsaturated membranes. (4) The cholesterol-induced increase is larger in DOPC membranes than that in DEPC membranes (which is much larger than in DSPC membranes).

The cholesterol effect in DLPC membranes can be explained by enhancement of the trans configuration of the alkyl chain

Table IV: Oxygen Permeability Coefficients for EYPC–Cholesterol Membranes

temp (°C)	cholesterol mole fraction (%)	D(water)[a] $(10^{-5}\ cm^2/s)$	P_W[b] (cm/s)	P_M/P_W[c] from pulse ESR	P_M[d] (cm/s)
0	0	1.12	34.9	0.43	15.0
	50	1.12	29.3	0.14	4.1
10	0	1.47	45.8	0.71	32.5
	50	1.47	38.5	0.30	11.6
40	0	3.30	102.8	1.96	201.5
	50	3.30	86.4	0.85	73.4

[a] The bulk diffusion coefficient of molecular oxygen in water. Data obtained from St.-Denis and Fell (1971). [b] Oxygen permeability coefficient across the water layer that has the same thickness as the membrane [calculated from the membrane thickness (δ_M) as determined below and D(water) according to eq 6]. [c] This ratio was determined from P_M and P_W, both of which are determined in the pulse ESR spin label experiment. [d] P_M was determined by multiplying P_W determined from the bulk diffusion coefficient and the P_M/P_W ratio determined by the present spin label method. In this way, ambiguities of p and r_0 can be avoided (see eq 2). The thickness of the membrane (δ_M) was published for EYPC membranes (Levine & Wilkins, 1971; Lis et al., 1982). The thickness of the hydrocarbon layer (δ_H) and that of the polar headgroup region (including the glycerol ester groups, δ_P) were calculated by the method of Cornell and Separovic (1983) assuming that the average volume of CH$_2$ groups obtained for DMPC membranes at 60 °C can be used for EYPC at 0–40 °C. This assumption can be justified by the observation in which the average volume asymptotically approaches a temperature- and chain-length-independent value above the main phase transition (Nagle & Wilkinson, 1978; Janiak et al., 1976, 1979). The additional assumptions are vol(CH$_3$) = 2vol(CH$_2$) (Nagle & Wilkinson, 1978), vol(CH) = vol(CH$_2$), and cholesterol does not affect the thickness of polar headgroup region (McIntosh, 1978). Obtained thicknesses are δ_H = 24.5 Å, δ_P = 3.8 Å, and δ_M = 32.1 Å for EYPC membranes; δ_H = 30.6 Å, δ_P = 3.8 Å, and δ_M = 38.2 Å for EYPC–50 mol % cholesterol membranes. It is assumed that the locations of the alkyl chain carbon atoms in the membrane change linearly with the position on the alkyl chain [the maximum error is about ±1.5 Å (Zaccai et al., 1979; Janiak et al., 1976)] and that the nitroxide group of SASL is located at the mean depth of 1- and 2-chain of PC.

and a better match in length between the bulky ring structure of cholesterol and the lauroyl chains.

From the above results 3 and 4, it is concluded that structural nonconformability between the rigid tetracyclic ring structure of cholesterol and the rigid bend at the C9–C10 double bond, the cis double bond in the oleoyl chains in particular, plays a key role in increasing $W(x)$ in the center of the bilayer. The structural nonconformability is more important than the mismatch in length.

Oxygen Permeability Across Unsaturated PC–Cholesterol Membranes. Oxygen permeability across the membrane (P_M) can be calculated from the $W(x)$ profiles in Figure 5 on the basis of a theory by Diamond and Katz (1974) [see eq 4 under Experimental Procedures; for the details of this calculation, see Subczynski et al. (1989)]. The P_M values determined directly from $W(x)$ according to eq 4 contain some uncertainty of A (= $8\pi p r_0$) in eqs 2 and 3. Since A is remarkably independent of solvent viscosity, temperature, hydrophobicity, and spin label species (Subczynski & Hyde, 1981, 1984; Hyde & Subczynski, 1984, 1989), the ratio of the permeability coefficient across the membrane (P_M) to the permeability across a water layer of the same thickness as the membrane [P_W, obtained from $W(d$-tempone) in Figure 5 according to eq 5] can be evaluated precisely by using the spin labeling T_1 method. The P_M/P_W ratios are shown as a function of cholesterol mole fraction and temperature in Figure 7. The cholesterol effect in unsaturated-PC membranes is much smaller than that in DMPC membranes (Subczynski et al., 1989).

It should be noted that incorporation of cholesterol decreases oxygen permeability in all membranes in spite of the increase in oxygen transport parameter in the center of the bilayer in unsaturated PC–cholesterol membranes. This is due to the fact that the major barrier for oxygen permeability across the membrane is located in T-PC and 5-SASL regions (Subczynski et al., 1989). In these regions, the presence of cholesterol decreases oxygen transport. Figure 7 also indicates that unsaturated PC membranes can be a moderate oxygen barrier only at high cholesterol concentrations at low temperatures.

The oxygen permeability coefficients for EYPC-cholesterol membranes can be determined by multiplying the P_M/P_W ratio determined as above and P_W determined from the macroscopic diffusion coefficient in the bulk water (St.-Denis & Fell, 1981) according to eq 6. These values are summarized in Table IV.
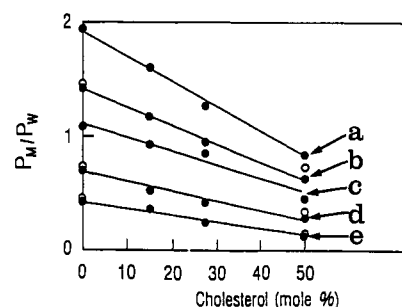

FIGURE 7: Oxygen permeability across the membrane (P_M) relative to that across a water layer of the same thickness as the membrane (P_W), P_M/P_W, for EYPC–cholesterol (●) and DOPC–cholesterol (○) membranes plotted as a function of the mole fraction of cholesterol. Temperature: 40 (a), 30 (b), 20 (c), 10 (d), and 0 (e) °C. Measurements for DOPC membranes were carried out at 30, 10, and 2 °C. Both P_M and P_W were obtained by the T_1 method. See the text and Table IV for details.

These numbers are comparable to those determined for DOPC-cholesterol membranes (Subczynski et al., 1989).

GENERAL DISCUSSION

The results on $W(x)$ obtained in the present work can be summarized as follows.

(1) In the absence of cholesterol, introduction of *either a cis or trans* double bond at C9–C10 position *decreases* the oxygen transport parameter at all locations (T-PC, 5-SASL, and 16-SASL) in the membrane (Table II).

(2) The activation energy for the translational diffusion of molecular oxygen evaluated in DMPC membranes in 5-SASL region is 4.3 kcal/mol, comparable to the activation energy theoretically estimated for kink migration (4.8 kcal/mol; Träuble, 1971) or C–C bond rotation of alkyl chains (3.1 kcal/mol; Pace & Chan, 1982) in the membrane (Figure 3 and Table III).

(3) Intercalation of cholesterol in saturated PC membranes reduces the oxygen transport parameter in T-PC and 5-SASL regions and little affects that in the 16-SASL region (Figures 4B and 6).

(4) Intercalation of cholesterol in unsaturated PC membranes also reduces the oxygen transport in T-PC and 5-SASL regions. In contrast, it *increases* the oxygen transport in the 16-SASL region (Figures 4A, 5, and 6).
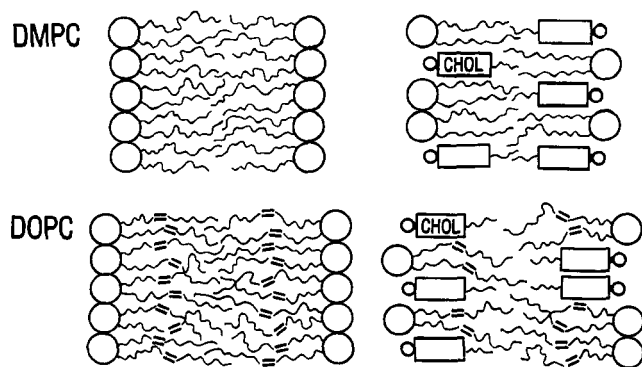
DMPC

CHOL

DOPC

CHOL

FIGURE 8: Schematic snapshot drawings of DMPC- and DOPC-cholesterol membranes, (left) without cholesterol; (right) with cholesterol. In DOPC membranes, two belted regions exist in which alkyl chain dynamics is suppressed due to the double bond. In DOPC-cholesterol membranes, nonconformability between the rigid bend at the cis double bond and the rigid sterol ring structure of cholesterol leads to formation of vacant pockets, increasing $W(16\text{-}SASL)$ in the central part of the bilayer.

On the basis of these observations, we propose a model for the molecular mechanism of oxygen transport in the membrane in which oxygen molecules reside in a vacant pocket created by the gauche–trans isomerization of alkyl chains and by the structural nonconformability of neighboring lipids and in which they jump from one pocket to the adjacent one or move along with the movement of the pocket itself (Figures 1 and 8).

The result (1) above is consistent with this model. Since there will be less motion around the double bond in the chain, either cis or trans unsaturation would decrease the oxygen transport in the double bond region. Intercalation of cholesterol (result 3) enhances the trans configuration of the single bond in the alkyl chain, decreasing the oxygen transport parameter.

The results (1, 2, and 3) thus indicate that dynamic gauche–trans isomerization of alkyl chains play an important role in oxygen diffusion in the membrane. Therefore, our data are consistent with the models proposed by Träuble (1971) and Pace and Chan (1982) in that the dynamics of gauche–trans isomerism is critically important. However, our result (4) indicates that the vacant pocket can be formed by structural non-conformability of adjacent lipids, enhanced by the mismatch in hydrophobic length. Involvement of the specific kink conformation may be in fact quite limited in unsaturated PC-cholesterol membranes (K. Kitamura and A. Kusumi, unpublished results).

The single most important observation in the present work would be the cholesterol-induced *increase* in the oxygen transport parameter in the central part of EYPC and DOPC membranes and also to a lesser extent in DEPC membranes (Figure 6). Due to (I) the structural nonconformability of the rigid bend at the cis double bond in the alkyl chain and the rigid plate-like steroid backbone of cholesterol, coupled with (II) the bulkiness of the steroid tetracyclic ring structure and (III) the mismatch in length between the alkyl chain and cholesterol, intercalation of cholesterol in unsaturated PC membranes would produce more and/or larger vacant pockets in the central region of the bilayer, as proposed previously (Subczynski et al., 1990), leading to enhanced oxygen transport in the central part. Therefore, the result (4) above is consistent with this model for the interaction of unsaturated PC and cholesterol and also with the model of vacant pocket-enhanced oxygen transport proposed above. These results and our model are summarized in Figure 8.

In our previous study on $CuKTSM_2$ transport in membranes, incorporation of cholesterol was found to decrease the

$CuKTSM_2$ transport parameter in the central part of the membrane but to a much less extent as compared to the decrease in T-PC and 5-SASL regions. Since oxygen molecules are much smaller than $CuKTSM_2$, the vacant pocket created in the central part of the membrane would be detected much more sensitively by oxygen molecules. Pharmacologically, these results suggest a possibility that hydrophobic drug molecules are much more concentrated in the central part of the membrane.

We would stress the importance of realizing the difference between the vacant pocket model for oxygen transport and the free volume model for phospholipid diffusion. Since oxygen molecules are small, small pockets created both intramolecularly and intermolecularly are sufficient for the residency and diffusion of molecular oxygen. In contrast, the larger free volume has to be created between the lipid molecules for the diffusion of larger molecules (Träuble & Sackmann, 1972; Galla et al., 1979; Pace & Chan, 1982; Peters & Cherry, 1982; Vaz et al., 1982, 1985; Shin et al., 1990).

The use of molecular oxygen as a membrane probe is unique in that it reports on the dynamic organization of the membrane at the submolecular level due to its small size. In addition, the membrane profile of the oxygen transport parameter clearly displays the three-dimensional fluidity and organization of the membrane. We took full advantage of these features of the oxygen transport parameter in this work. We are in the process of extending the use of the oxygen transport parameter to the reconstituted membranes of proteins and lipids and biological membranes.

Can the Membrane Affect the Oxygen Consumption Rate of the Cell by Becoming a Barrier for Oxygen Permeability? Since the apparent Michaelis constant K_m for the oxygen consumption by the cell or by the mitochondrion was found to be in the range of 0.1–1 μM (Degn & Wohlrab, 1971; Petersen et al., 1974; Wilson et al., 1979, 1988; Lai et al., 1982) and the oxygen concentration under hypoxic conditions in vivo may be in the order of micromolar, a possibility is discussed here in which changes in the oxygen permeability of the membrane can affect and control the oxygen consumption rate in the cell or in the mitochondrion. Boag (1969) showed that the following equations describe the spatial profile of oxygen concentration outside and inside a spherical cell (or a mitochondrion), assuming uniform consumption of oxygen inside the cell (or the mitochondrion).

$$C(r) = C_\infty - V/4\pi RD(R/r) \qquad r \geq R \qquad (7)$$

$$C(r) = C_\infty - 3V/8\pi RD(1 - r^2/3R^2) \qquad r < R \qquad (8)$$

where R is the radius of the cell (mitochondrion), V the oxygen consumption rate, and D the diffusion coefficient of molecular oxygen (assuming that D in the cell is the same as that outside of the cell). On the basis of these equations, the gradient of oxygen concentration, ΔC, can be calculated:

$$\Delta C_1 =$$
$$V/4\pi RD \text{ from infinite distance to the cell membrane} \quad (9)$$

$$\Delta C_2 = V/8\pi RD \text{ from the cell membrane to the center of the cell} \quad (10)$$

The oxygen gradient across the cell membrane can be estimated as

$$\Delta C_M =$$
$$\text{(the flux of molecular oxygen at the membrane)}/P_M$$
$$(11)$$

(see Figure 9). The flux of molecular oxygen can be calcu-

Table V: Predicted Oxygen Concentration Gradients (μM) Calculated for a Suspended Cell or a Mitochondrion for Four Models of Oxygen Permeability Coefficients Across the Membrane[a]

	cells[b]			mitochondrion[c]		
P_M	ΔC_1	ΔC_2	ΔC_M	ΔC_1	ΔC_2	ΔC_M
$P_M = P_W$	0.2	0.1	0.00012	0.4	0.2	0.002
$P_M = 0.1P_W$	0.2	0.1	0.0012	0.4	0.2	0.02
$P_M = 0.01P_W$	0.2	0.1	0.012	0.4	0.2	0.2
$P_M = 0.0001P_W$	0.2	0.1	1.2	0.4	0.2	20.0

[a] The measured values of P_M for PC–cholesterol bilayers are in the range of 0.1–1 $\times$ P_W, suggesting that P_M for biological membranes containing proteins may be in the range of 0.01–1 $\times$ P_W. The concentration gradients outside the cell, $\Delta C_1 = V/4\pi RD$ (from infinite distance to the cell membrane), inside the cell, $\Delta C_2 = V/8\pi RD$ (from the cell membrane to the center of the cell), and across the membrane, $\Delta C_M =$ (the flux of molecular oxygen at the membrane)$/P_M$ were estimated. See the text and Figure 10 for details. The diffusion coefficient of molecular oxygen used was $D = 3 \times 10^{-5}$ cm^2/s [at 37 °C (St.-Denis & Fell, 1971)] and $P_W = 60$ cm/s ($\delta_M = 50$ Å). When these gradients are comparable to C_∞ or K_m, these estimates are no longer correct. Nevertheless, this table provides a convenient guideline to evaluate the contribution of the membrane to the concentration gradient of molecular oxygen. [b] The calculation for the cell was made for Chinese hamster ovary cells of the mean radius $R = 8.2$ μm (Lai et al., 1980) and the mean oxygen consumption rate $V = 6 \times 10^{-17}$ mol of O_2 per second per cell (Lai et al., 1982). Comparable oxygen consumption rate was reported for other cells (Froese, 1962; Boag, 1969; Wittenberg & Wittenberg, 1985). [c] The calculation is based on the values for muscle mitochondria of $R = 1$ μm and $V = 1.5 \times 10^{-17}$ mol of O_2 per second per mitochondrion (Hoppeler & Lindstedt, 1985; Hoppeler et al., 1987).
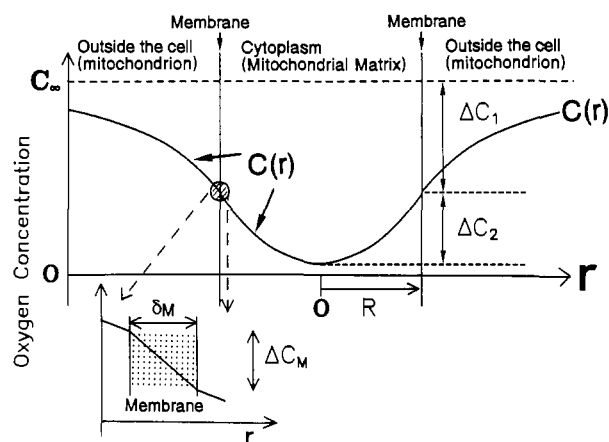

FIGURE 9: Profile of oxygen concentration around a cell (mitochondrion) assuming uniform oxygen consumption by the cell (mitochondrion, radius R). Three regions are considered separately (eqs 7–11): (1) from infinite distance to the cell membrane, $\Delta C_1 = V/4\pi RD$; (2) from the cell membrane to the center of the cell, $\Delta C_2 = V/8\pi RD$; (3) the oxygen gradient across the membrane, $\Delta C_M =$ (the flux of molecular oxygen at the membrane)$/P_M$. The figure indicates that ΔC_M for the plasma membrane is not comparable to ΔC_1 or ΔC_2 if P_M for the plasma membrane is close to P_M for EYPC membranes listed in Table IV. See the text and Table V for details.

lated from the oxygen consumption rate of the cell and the surface area of the cell. Estimated values for ΔC_1, ΔC_2, and ΔC_M are summarized in Table V for four models: (1) $P_M = P_W$ for the PC $\pm$ cholesterol membrane in the liquid-crystalline phase at physiological temperatures; (2) $P_M = 0.1P_W$ for the 50 mol % cholesterol–PC membrane at low temperatures (0–4 °C); (3) $P_M = 0.01P_W$, the smallest P_M, which may be observed in protein-rich membranes such as the purple membrane in *Halobacterium halobium* (I. Ashikawa, W. K. Subczynski, and A. Kusumi, unpublished observation); and (4) $P_M = 0.0001P_W$, a hypothetical case, in which oxygen permeability of the membrane is very low and rate limiting for oxygen consumption in the cell.

We would expect that P_M for the mitochondrial membrane is between $0.1P_W$ and $0.01P_W$ because it contains a high concentration of membrane proteins and the oxygen transport parameter in proteins is small [1/60 of that in water in the case of the β-ionone binding site in rhodopsin (Subczynski et al., 1991)]. The model calculation summarized in Table V thereby indicates that the oxygen permeability of the mitochondrial membranes can limit or regulate the oxygen consumption rate in mitochondria. In addition, oxygen permeability of the mitochondrial membrane may be important when

the oxygen consumption rate is very high (Neely et al., 1967). This result thus presents an interesting challenge for measurements of oxygen permeability across the mitochondrial membranes and oxygen concentration gradients in vivo.

CONCLUSIONS

(1) We propose a model for the molecular mechanism of oxygen transport in the membrane in which oxygen molecules reside in vacant pockets and jump from one pocket to the adjacent pocket or move along with the movements of the pocket itself. These vacant pockets are created by gauche–trans isomerization of alkyl chains and by packing defects in membranes caused by the structural nonconformability and the mismatch in length between neighboring lipids.

(2) In the absence of cholesterol, incorporation of *either cis or trans* double bond at the C9–C10 position of the alkyl chain decreases the oxygen transport parameter at all locations in the membrane. This result can be explained by the formation in the membrane of the region in which gauche–trans isomerization is significantly suppressed by the presence of double bonds in high concentrations, which, according to the above model, would decrease the oxygen transport.

(3) The structural nonconformability of the rigid ring system of cholesterol and the rigid bend at the cis double bond in the unsaturated alkyl chain, coupled with the mismatch in hydrophobic length between cholesterol (the bulky fused-ring structure of cholesterol in particular) and PC, would lead to create more and/or larger vacant pockets in the central region of the bilayer in unsaturated PC–cholesterol membranes. This, in turn, would lead to an increase of oxygen transport and an enhancement of some motional modes of 16-SASL in the middle of the bilayer.

(4) In saturated PC membranes, intercalation of cholesterol reduces the oxygen transport parameter in T-PC and 5-SASL regions by enhancing the trans configuration, thus reducing the gauche–trans isomerization, of the alkyl chain. Little influence of cholesterol in the 16-SASL region may be explained by cancellation of the two opposite effects: enhancement of trans configuration of alkyl chains that are in contact with the cholesterol ring structure and formation of vacant pockets in the middle of the bilayer. The vacant pockets may be filled with nearby alkyl chains.

(5) Incorporation of cholesterol decreases the oxygen transport parameter in and near the headgroup region in all membranes. Since the major barrier for oxygen permeability across the membrane is located in this region, the presence of cholesterol decreases oxygen permeability in all membranes

used in this work in spite of the increase in oxygen transport parameter in the center of the bilayer in unsaturated PC-cholesterol membranes.

(6) We suggest that the effect of alkyl chain unsaturation (USE) on transport of small molecules and alkyl chain dynamics in the membranes is determined by the interplay of the following factors. (USE1) Because of the rigidity of the double bond, the alkyl chain dynamics is reduced around the double bond. (USE2) The rigid bend at the double bond makes packing of alkyl chains less efficient, decreasing the phase-transition temperature drastically. (USE3) The rigid bend at the double bond and the rigid tetracyclic ring of cholesterol do not conform to each other, enhancing the formation of vacant pockets and cholesterol-rich (cholesterol-oligomeric) domains in the membrane.

(7) The mitochondrial membranes can be a limiting barrier for oxygen consumption under hypoxic conditions in vivo.

References

Adam, G., & Delbrück, M. (1968) in *Structural Chemistry and Molecular Biology* (Davidson, N., & Rich, A., Eds.) pp 198–215, Freeman, San Francisco, CA.

Albert, B., Bray, D., Lewis, J., Raff, M., Roberts, K., & Watson, J. D. (1988) *Molecular Biology of the Cell*, 2nd ed., pp 300–304, Garland, New York.

Anderson, O. S. (1978) in *Membrane Transport in Biology* (Giebisch, G., Tosteson, D. C., & Ussing, H. H., Eds.) Vol. 1, pp 369–446, Springer, New York.

Boag, J. W. (1969) *Curr. Top. Radiat. Res. 5*, 141–195.

Cornell, B. A., & Separovic, F. (1983) *Biochim. Biophys. Acta 733*, 189–193.

Curatro, W., Sakura, J. D., Small, D. M., & Shipley, G. G. (1977) *Biochemistry 16*, 2313–2319.

Degn, H., & Wohlrab, H. (1971) *Biochim. Biophys. Acta 245*, 347–355.

Demel, R. A., & de Kruyff, B. (1976) *Biochim. Biophys. Acta 457*, 109–132.

Diamond, J. M., & Katz, Y. (1974) *J. Membr. Biol. 17*, 121–154.

Egret-Charlier, M., Sanson, A., Ptak, M., & Bouloussa, O. (1978) *FEBS Lett. 87*, 313–316.

Feix, J. B., Yin, J.-J., & Hyde, J. S. (1987) *Biochemistry 26*, 3850–3855.

Finkelstein, A. (1984) *Curr. Top. Membr. Trans. 21*, 295–308.

Franks, N. P., & Lieb, W. R. (1979) *J. Mol. Biol. 133*, 469–500.

Froese, G. (1962) *Biochim. Biophys. Acta 57*, 509–519.

Galla, H. J., Hartmann, W., Theilen, U., & Sackmann, E. (1979) *J. Membr. Biol. 48*, 215–236.

Hoppeler, H., & Lindstedt, S. L. (1985) *J. Exp. Biol. 115*, 355–364.

Hoppeler, H., Kayar, S. R., Claassen, H., Uhlmann, E., & Karas, R. H. (1987) *Respir. Physiol. 69*, 27–46.

Huisjen, M., & Hyde, J. S. (1974) *Rev. Sci. Instrum. 45*, 669–675.

Hyde, J. S., & Subczynski, W. K. (1984) *J. Magn. Reson. 56*, 125–130.

Hyde, J. S., & Subczynski, W. K. (1989) in *Biological Magnetic Resonance, Spin Labeling: Theory and Appli-*

cations (Berliner, L. J., & Reuben, J., Eds.) Vol. 8, pp 399–425, Plenum, New York.

Ipsen, J. H., Karlstrom, G., Mouritsen, O. G., Wennerstrom, H., & Zuckermann, M. J. (1987) *Biochim. Biophys. Acta 905*, 162–172.

Janiak, M. J., Small, D. M., & Shipley, G. G. (1976) *Biochemistry 15*, 4575–4580.

Janiak, M. J., Small, D. M., & Shipley, G. G. (1979) *J. Biol. Chem. 254*, 6068–6078.

Jain, M. K., & Wagner, R. F. (1980) in *Introduction to Biological Membranes*, Wiley, New York.

Kusumi, A., & Hyde, J. S. (1982) *Biochemistry 21*, 5978–5983.

Kusumi, A., & Pasenkiewicz-Gierula, M. (1988) *Biochemistry 27*, 4407–4415.

Kusumi, A., Subczynski, W. K., & Hyde, J. S. (1982a) *Proc. Natl. Acad. Sci. U.S.A. 79*, 1854–1858.

Kusumi, A., Subczynski, W. K., & Hyde, J. S. (1982b) *Fed. Proc. 41*, 1394, Abstract 6571.

Kusumi, A., Tsuda, M., Akino, T., Ohnishi, S., & Terayama, Y. (1983) *Biochemistry 22*, 1165–1170.

Kusumi, A., Subczynski, W. K., Pasenkiewicz-Gierula, M., Hyde, J. S., & Merkle, H. (1986) *Biochim. Biophys. Acta 854*, 307–317.

Lai, C.-S., Hopwood, L. E., & Schwartz, H. M. (1980) *Biochim. Biophys. Acta 602*, 117–126.

Lai, C.-S., Hopwood, L. E., Hyde, J. S., & Lukiewicz, S. (1982) *Proc. Natl. Acad. Sci. U.S.A. 79*, 1854–1858.

Levine, Y. K., & Wilkins, M. H. F. (1971) *Nature (London), New Biol. 230*, 69–72.

Lis, L. J., McAlister, M., Fuller, N., Rand, R. P., & Parsegian, V. A. (1982) *Biophys. J. 37*, 657–666.

McIntosh, T. J. (1978) *Biochim. Biophys. Acta 513*, 43–58.

Merkle, H., Subczynski, W. K., & Kusumi, A. (1987) *Biochim. Biophys. Acta 897*, 238–248.

Nagle, J. F., & Wilkinson, D. A. (1978) *Biophys. J. 23*, 159–175.

Neely, J. R., Libermeister, H., Battersby, E. J., & Morgan, H. E. (1967) *Am. J. Physiol. 195*, 804–814.

Oldfield, E., Meadows, M., Rice, D., & Jacobs, R. (1978) *Biochemistry 17*, 2727–2740.

Pace, R. J., & Chan, S. I. (1982) *J. Chem. Phys. 76*, 4241–4247.

Pasenkiewicz-Gierula, M., Subczynski, W. K., & Kusumi, A. (1990) *Biochemistry 29*, 4059–4069.

Peters, R., & Cherry, R. J. (1982) *Proc. Natl. Acad. Sci. U.S.A. 79*, 4317–4321.

Petersen, L. C., Nicolls, P., & Degn, H. (1974) *Biochem. J. 142*, 247–252.

Presti, F. T. (1985) in *Membrane Fluidity in Biology* (Aloia, R. C., & Boggs, J. M., Eds.) Vol. 4, pp 97–146, Academic, New York.

Presti, F. T., & Chan, S. I. (1982) *Biochemistry 21*, 3821–3830.

Presti, F. T., Pace, R. J., & Chan, S. I. (1982) *Biochemistry 21*, 2831–2835.

Recktenwald, D. J., & McConnell, H. M. (1981) *Biochemistry 20*, 4505–4510.

Sanson, A., Ptak, M., Rignaud, J. L., & Gary-Bobo, C. M. (1976) *Chem. Phys. Lipids 17*, 435–444.

Seelig, J., & Waespa-Šarčevič, N. (1978) *Biochemistry 17*, 3310–3315.

Shin, Y.-K., & Freed, J. F. (1989a) *Biophys. J. 55*, 537–550.

Shin, Y.-K., & Freed, J. F. (1989b) *Biophys. J. 56*, 1093–1100.

Shin, Y.-K., & Moscicki, J. K., & Freed, J. H. (1990) *Biophys. J. 57*, 445–459.

Small, D. M. (1967) *J. Lipid Res. 8*, 551–557.

Smotkin, E. S., Moy, F. T., & Plachy, W. Z. (1991) *Biochim. Biophys. Acta* (in press).

St.-Denis, C. E., & Fell, C. J. D. (1971) *Can. J. Chem. Eng. 49*, 885.

Subczynski, W. K. (1984) *Zeszyty Nauk. Uniw. Jagiellon. 10*, 145–203 (in Polish).

Subczynski, W. K., & Hyde, J. S. (1981) *Biochim. Biophys. Acta 643*, 283–291.

Subczynski, W. K., & Hyde, J. S. (1983) *Biophys. J. 41*, 283–286.

Subczynski, W. K., & Hyde, J. S. (1984) *Biophys. J. 45*, 743–748.

Subczynski, W. K., & Kusumi, A. (1986) *Biochim. Biophys. Acta 854*, 318–320.

Subczynski, W. K., Antholine, W. E., Hyde, J. S., & Petering, D. H. (1987) *J. Am. Chem. Soc. 109*, 46–52.

Subczynski, W. K., Hyde, J. S., & Kusumi, A. (1989) *Proc. Natl. Acad. Sci. U.S.A. 86*, 4474–4478.

Subczynski, W. K., Antholine, W. A., Hyde, J. S., & Kusumi, A. (1990) *Biochemistry 29*, 7936–7945.

Subczynski, W. K., Renk, G., Crouch, R., Hyde, J. S., & Kusumi, A. (1991) *Biophys. J.* (submitted).

Tinker, D. O., Pinteric, L., Hsia, J. C., & Rand, R. P. (1976) *Can. J. Biochem. 54*, 209–218.

Träuble, H. (1971) *J. Membr. Biol. 4*, 193–208.

Träuble, H., & Sackmann, E. (1972) *J. Am. Chem. Soc. 94*, 4499–4510.

Träuble, H., & Eibl, H. (1974) *Proc. Natl. Acad. Sci. U.S.A. 71*, 214–219.

Vaz, W. L. C., Criado, M., Madeira, V. M. C., Schoellmann, G., & Jovin, T. M. (1982) *Biochemistry 21*, 5608–5612.

Vaz, W. L. C., Clegg, R. M., & Hallmann, D. (1985) *Biochemistry 24*, 781–786.

Vist, M. R., & Davis, J. H. (1990) *Biochemistry 29*, 451–464.

Walter, A., & Gutknecht, J. (1986) *J. Membr. Biol. 90*, 207–217.

Wilson, D. F., Erecinska, M., Drown, C., & Silver, J. A. (1979) *Arch. Biochem. Biophys. 195*, 485–493.

Wilson, D. F., Rumsey, W. L., Green, T. J., & Vanderkooi, J. M. (1988) *J. Biol. Chem. 263*, 2712–2718.

Wittenberg, B. A., & Wittenberg, J. B. (1985) *J. Biol. Chem. 260*, 6548–6554.

Yeagle, P. L. (1985) *Biochim. Biophys. Acta 822*, 267–287.

Yeagle, P. L. (1988) *Biology of Cholesterol*, CRC Press, Boca Raton, FL.

Yin, J.-J., & Hyde, J. S. (1987) *Z. Phys. Chem. (Munich) 153*, 541–549.

Yin, J.-J., Pasenkiewicz-Gierula, M., & Hyde, J. S. (1987) *Proc. Natl. Acad. Sci. U.S.A. 79*, 1854–1858.

Zaccai, G., Buldt, G., Seelig, A., & Seelig, J. (1979) *J. Mol. Biol. 134*, 693–706.

Mechanism of DNA Polymerase α Inhibition by Aphidicolin[†,‡]

Robert Sheaff, Diane Ilsley, and Robert Kuchta*

Department of Chemistry and Biochemistry, University of Colorado, Boulder, Colorado 80309-0215

Received March 18, 1991; Revised Manuscript Received June 14, 1991

ABSTRACT: Synthetic oligonucleotides of defined sequence were used to examine the mechanism of calf thymus DNA polymerase α inhibition by aphidicolin. Aphidicolin competes with each of the four dNTPs for binding to a pol α·DNA binary complex and thus should not be viewed as a dCTP analogue. Kinetic evidence shows that inhibition proceeds through the formation of a pol α·DNA·aphidicolin ternary complex, while DNase I protection experiments provide direct physical evidence. When deoxyguanosine is the next base to be replicated, $K_i = 0.2\ \mu M$. In contrast, the K_i is 10-fold higher when the other dNMPs are at this position. Formation of a pol α·DNA·aphidicolin ternary complex did not inhibit the primase activity of the pol α·primase complex. Neither the rate of primer synthesis nor the size distribution of primers 2–10 nucleotides long was changed. Elongation of the primase-synthesized primers by pol α was inhibited both by ternary complex formation using exogenously added DNA and by aphidicolin alone.

Aphidicolin, a tetracyclic diterpenoid isolated from *Cephalosporium aphidicola* (Brundret et al., 1972), is a potent inhibitor of DNA replication (Bucknall et al., 1973). It specifically inhibits polymerase α (Spadari et al., 1982) and was found to inhibit mitotic division of sea urchin embryos while not affecting nondividing cells (Ikegami et al., 1978; Oguro et al., 1979). The drug proved to be instrumental in

identifying pol α[1] as a major eukaryotic replicative polymerase (Huberman, 1981). Aphidicolin also specifically inhibits pol δ (Byrnes, 1984), the α-like polymerase of plant cells, and the herpes simplex virus and vaccinia virus encoded DNA polymerases (Pedrali-Noy & Spadari, 1980a; Huberman, 1981; Spadari et al., 1982, 1984, 1985a,b; Fry & Loeb 1986), while not affecting DNA methylation or RNA, protein, and nucleotide biosynthesis (Spadari et al., 1982, 1984, 1985a). This

[1] Abbreviations: Aph, aphidicolin; EDTA, ethylenediaminetetraacetic acid (sodium salt); pol α, DNA polymerase α:primase; pol δ, DNA polymerase δ; Tris, tris(hydroxymethyl)aminomethane (HCl salt).